



# Retrieval of three-dimensional small-scale structures in upper-tropospheric/lower-stratospheric composition as measured by GLORIA

M. Kaufmann<sup>1</sup>, J. Blank<sup>1,\*</sup>, T. Guggenmoser<sup>1</sup>, J. Ungermann<sup>1</sup>, A. Engel<sup>6</sup>, M. Ern<sup>1</sup>, F. Friedl-Vallon<sup>2</sup>, D. Gerber<sup>4</sup>, J. U. Groß<sup>1</sup>, G. Guenther<sup>1</sup>, M. Höpfner<sup>2</sup>, A. Kleinert<sup>2</sup>, E. Kretschmer<sup>2</sup>, Th. Latzko<sup>2</sup>, G. Maucher<sup>2</sup>, T. Neubert<sup>8</sup>, H. Nordmeyer<sup>2</sup>, H. Oelhaf<sup>2</sup>, F. Olschewski<sup>3</sup>, J. Orphal<sup>2</sup>, P. Preusse<sup>1</sup>, H. Schlager<sup>7</sup>, H. Schneider<sup>8</sup>, D. Schuettmeyer<sup>5</sup>, F. Stroh<sup>1</sup>, O. Suminska-Ebersoldt<sup>2</sup>, B. Vogel<sup>1</sup>, C. M. Volk<sup>3</sup>, W. Woiwode<sup>2</sup>, and M. Riese<sup>1</sup>

<sup>1</sup>Institute of Energy and Climate Research, Stratosphere (IEK-7), Research Centre Jülich, 52425 Jülich, Germany

<sup>2</sup>Institute for Meteorology and Climate Research, Karlsruhe Institute of Technology, Karlsruhe, Germany

<sup>3</sup>Physics Department, University of Wuppertal, 42097 Wuppertal, Germany

<sup>4</sup>RAL Space, STFC Rutherford Appleton Laboratory, Harwell Oxford, Didcot, OX11 0QX, UK

<sup>5</sup>European Space Agency, Mission Science Division, 2200AG Noordwijk, the Netherlands

<sup>6</sup>Institute for Atmospheric and Environmental Sciences, Goethe University Frankfurt, 60438 Frankfurt am Main, Germany

<sup>7</sup>German Aerospace Center, Institute of Atmospheric Physics, Atmospheric Trace Species, 82234 Oberpfaffenhofen-Wessling, Germany

<sup>8</sup>Central Institute of Engineering, Electronics and Analytics (ZEA-2) – Electronic Systems, Research Centre Jülich, Jülich, Germany

\* now at: Google Inc., Dublin, Ireland

Correspondence to: M. Kaufmann (m.kaufmann@fz-juelich.de)

Received: 17 March 2014 – Published in Atmos. Meas. Tech. Discuss.: 29 April 2014

Revised: 2 October 2014 – Accepted: 20 October 2014 – Published: 9 January 2015

**Abstract.** The three-dimensional quantification of small-scale processes in the upper troposphere and lower stratosphere is one of the challenges of current atmospheric research and requires the development of new measurement strategies. This work presents the first results from the newly developed Gimballed Limb Observer for Radiance Imaging of the Atmosphere (GLORIA) obtained during the ESSenCe (ESA Sounder Campaign) and TACTS/ESMVal (TACTS: Transport and composition in the upper troposphere/lowermost stratosphere, ESMVal: Earth System Model Validation) aircraft campaigns. The focus of this work is on the so-called dynamics-mode data characterized by a medium-spectral and a very-high-spatial resolution. The retrieval strategy for the derivation of two- and three-dimensional constituent fields in the upper troposphere and lower stratosphere is presented. Uncertainties of the main retrieval targets (temperature, O<sub>3</sub>, HNO<sub>3</sub>, and CFC-12) and their spatial resolution are discussed. During ESSenCe, high-resolution two-dimensional cross-sections have been ob-

tained. Comparisons to collocated remote-sensing and in situ data indicate a good agreement between the data sets. During TACTS/ESMVal, a tomographic flight pattern to sense an intrusion of stratospheric air deep into the troposphere was performed. It was possible to reconstruct this filament at an unprecedented spatial resolution of better than 500 m vertically and 20 × 20 km horizontally.

## 1 Introduction

The upper troposphere and lower stratosphere has gained increasing attention in recent years due to their importance in the climate system (Solomon et al., 2007; Riese et al., 2012). Quantifying the structure and chemical composition to understand the underlying physical processes are current topics of atmospheric research. The quantification of small-scale structures and dynamical processes is a key topic for the

understanding of this atmospheric region (Gettelman et al., 2011) because cross-tropopause transport and mixing around jet streams give an important contribution to stratosphere–troposphere exchange (e.g., Manney et al., 2011; Seo and Bowman, 2002; Olsen et al., 2008) and affect the mixing layers above the tropopause (e.g., Hoor et al., 2002).

Satellite-borne limb observations have enhanced our understanding of the three-dimensional chemical structure and large-scale dynamics of the middle atmosphere significantly in recent years. Our knowledge of small-scale structures is, however, primarily based on in situ observations by means of research aircraft and high-altitude balloons. Airborne limb-emission sensors such as CRISTA-NF (CRyogenic Infrared Spectrometers and Telescopes for the Atmosphere – New Frontiers; Weigel et al., 2012; Ungermann et al., 2013) and MIPAS-STR (Michelson Interferometer for Passive Atmospheric Sounding – STRatospheric Aircraft, Piesch et al., 1996; Woiwode et al., 2012) complemented the satellite and in situ data with their high spatial sampling in two dimensions (vertical and along the flight track).

The quantification of small-scale processes in all three dimensions requires the development of new instruments and new measurement strategies. Ungermann et al. (2010) presented a new approach to obtain trace gas filaments and temperature fluctuations by means of airborne remote sounding utilizing tomographic reconstruction techniques. The two key factors for this measurement strategy are closed or nearly closed flight paths (diameter of a few hundred kilometers) and the ability to make measurements from different viewing angles with respect to the aircraft position.

The Gimballed Limb Observer for Radiance Imaging of the Atmosphere (GLORIA; Riese et al., 2014; Friedl-Vallon et al., 2014) is a newly developed instrument for delivering data for such kinds of tomographic reconstruction. It can measure images of mid-infrared limb emission spectra within a few seconds and has the capability to pan its line of sight from 48 to 118° with respect to the aircraft nose.

This work describes results from the first two deployments of the GLORIA instrument, namely during ESSenCe (ESa Sounder Campaign; Kaufmann et al., 2013) and during the TACTS/ESMVal campaign (TACTS: Transport and composition in the upper troposphere/lowermost stratosphere, ESMVal: Earth System Model Validation). The former campaign was conducted to perform a first in-flight testing of the GLORIA instrument and to verify the GLORIA retrieval products. In the latter campaign, several closed flight paths were performed to allow for the application of tomographic reconstruction techniques to real GLORIA measurements for the first time.

The outline of this paper is as follows: After a short description of the GLORIA instrument (Sect. 2), we describe the retrieval strategy for the GLORIA so-called dynamics-mode measurements (Sect. 3) including a short review of the forward and inverse model. Section 4 gives an overview of the ESSenCe campaign and presents the first GLORIA mea-

surements including a discussion of their uncertainties, vertical resolution, and a comparison with collocated measurements and simulations. The first tomographic measurements of a filamentary structure during the TACTS/ESMVal campaign are presented in Sect. 5.

## 2 GLORIA Instrument

GLORIA is an infrared limb sounder which combines the high horizontal resolution of a nadir sounder (tens of kilometers) with the altitude resolution provided by a limb-sounding instrument. The purpose of GLORIA is to measure temperature and composition in the upper troposphere/lower stratosphere at high spatial resolution (Riese et al., 2014). This is achieved by mounting an imaging Michelson interferometer with a high-resolution two-dimensional infrared detector onto a gimbal, allowing it to point and stabilize the instrument in the azimuthal, elevational, and image rotation directions (Friedl-Vallon et al., 2014). It is designed to be deployed on board different research aircraft, namely the Russian high-altitude research aircraft M55 Geophysica and the German High Altitude and Long Range (HALO) research aircraft.

GLORIA is able to measure infrared limb or nadir emissions between 780 and 1400  $\text{cm}^{-1}$ . The limb images cover a vertical field of view of 0.8 to  $-3.3^\circ$  with respect to the horizontal;  $-3.3^\circ$  corresponds to a lower tangent altitude of about 4 km. The field of view can be pointed about  $10^\circ$  upward as a quasi-deep space view and into two large area blackbodies for radiometric calibration (Olschewski et al., 2013).

Tomographic measurements are performed in the so-called dynamics mode. In this mode, GLORIA operates at low optical path differences to obtain more spectra at a given time. During ESSenCe, GLORIA recorded spectra at a maximum optical path difference of 1.6 cm in 2.8 s for a pair of forward/backward spectra, yielding a spectral sampling of 0.3125  $\text{cm}^{-1}$ . During TACTS/ESMVal, dynamics-mode spectra were recorded at a maximum optical path difference of 0.8 cm in 2 s for a pair of forward/backward spectra, yielding a spectral sampling of 0.625  $\text{cm}^{-1}$ . Another measurement mode is the so-called chemistry mode with a spectral sampling of 0.0625  $\text{cm}^{-1}$  and 12 s measurement time. GLORIA data recorded in chemistry mode were analyzed by Woiwode et al. (2014). Individual GLORIA images contain  $128 \times 48$  pixel/spectra. The horizontal resolution of the detector array is used to analyze and filter cloud fractions. After filtering, the spectra are averaged horizontally on a  $128 \times 1$  grid for further processing. Different viewing angles of the same air mass are obtained by pointing the instrument from 48 to 118° (in  $4^\circ$  steps) with respect to the aircraft nose in a short time frame. The data obtained in this way can be combined and processed in a tomographic way to get a three-dimensional picture of the atmosphere.

### 3 Data Processing

When operating the GLORIA instrument during field measurement, raw interferograms and housekeeping data are written to a mass storage for later processing. The data rate is about 1 Gbit s<sup>-1</sup>. In the laboratory, this data is processed in several steps, including different calibration procedures and the retrieval of atmospheric temperature, trace gases, etc. These steps and the corresponding data level products are described below.

#### 3.1 Level 0 and Level 1

The Level 0 and Level 1 processing transforms the measured raw interferograms into radiometrically and spectrally calibrated spectra. The core of the Level 0 processing is the re-sampling of the interferograms. The raw interferograms are sampled on a time-equidistant grid. Before Fourier transformation, they have to be interpolated onto a space-equidistant grid, taking velocity variations of the interferometer drive into account. The Level 0 processing also includes a quality check of the data, spike detection and correction, non-linearity correction, correction of phase errors, and the spectral calibration. The Level 1 processing comprises the Fourier transform converting the interferograms to complex spectra and the radiometric calibration. Calibration spectra are generated from blackbody and quasi-deep space measurements using a two-point calibration. Details about the Level 0 and Level 1 processing of GLORIA data are given in Kleinert et al. (2014).

#### 3.2 Level 2

Level 2 processing encompasses the derivation of atmospheric or instrumental parameters from calibrated radiance measurements. This is performed in an iterative way by minimizing the difference between a forward model mapping of the atmospheric state to radiances as they would have been observed by the instrument and real GLORIA measurements. This minimization is performed by the so-called inversion model.

##### 3.2.1 Forward Modeling

The forward model consists of a radiative transfer and an instrument model. The radiative transfer model is based on a combination of the emissivity growth approximation (EGA; Gordley and Russell, 1981) and the Curtis–Godson approximation (CGA; Curtis, 1952; Godson, 1953). Both methods are based on pre-calculated emissivities of homogeneous gas cells for a variety of atmospheric conditions and pre-defined spectral ranges. The spectral ranges are either individual spectral points or integrated spectral windows combining several spectral points (Riese et al., 1997, 1999). The optical paths have been calculated by means of the line-by-line Reference Forward Model (RFM, Dudhia, 2000) uti-

lizing the HITRAN (High Resolution Transmission)-2012 spectral database (Rothman et al., 2013). The speed up of this method is up to a factor of thousand in comparison to a line-by-line model, and the uncertainties arising from the approximations are generally less than 1 % (Marshall et al., 1994; Francis et al., 2006; Ungermann et al., 2013).

The second part of the forward model is the instrument model. It maps various line-of-sight radiances onto the detector array. To consider field of view effects, several line-of-sight radiances are typically combined to simulate one or more detector pixel.

The retrieval of atmospheric quantities requires the calculation of the Jacobian of the forward model (see next section). This is done by algorithmic differentiation (Lotz et al., 2011; Ungermann et al., 2011), which is highly efficient in our case, because the computational costs for calculating the Jacobian matrix are only a constant multiple of a single execution of the forward model.

##### 3.2.2 Inverse Modeling

The reconstruction of an atmospheric state compatible with a sequence of GLORIA measurements is a nonlinear inversion problem. This is solved by minimizing a cost function  $\sigma_y$  describing the difference between the forward model  $F: \mathbb{R}^n \rightarrow \mathbb{R}^m$  of an atmospheric state  $\mathbf{x} \in \mathbb{R}^n$  (temperature, trace gas abundance, etc.) and the radiance measurement  $\mathbf{y} \in \mathbb{R}^m$ :

$$\sigma_y = (\mathbf{F}(\mathbf{x}) - \mathbf{y})^T \mathbf{S}_\epsilon^{-1} (\mathbf{F}(\mathbf{x}) - \mathbf{y}). \quad (1)$$

The difference is weighted by the inverse measurement error/error covariance matrix  $\mathbf{S}_\epsilon^{-1}$ . In most cases, the solution is not unique and/or under-constrained. Therefore, it has been proven useful to add a regularization term to the cost function:

$$\sigma_x = (\mathbf{x} - \mathbf{x}_a)^T \mathbf{L}^T \mathbf{L} (\mathbf{x} - \mathbf{x}_a). \quad (2)$$

In our case,  $\mathbf{L}$  is a Tikhonov-type matrix applying zero- and first-order difference operators (Twomey, 1977). A zero-order Tikhonov regularization constrains the absolute value, while the first-order minimizes the derivative in order to smooth the solution.  $\mathbf{x}_a$  describes a priori information about the atmospheric state.  $\mathbf{x}$  and  $\mathbf{x}_a$  may also contain parameters of the instrument model, such as a radiance offset. The definition of the a priori data and the regularization matrix  $\mathbf{L}$  depends on the atmospheric conditions and the instrument performance and is described later (Sect. 4.3.1).

The overall cost function is then  $\sigma = \sigma_y + \sigma_x$ , which is minimized using a truncated quasi-Newton minimizer. For three-dimensional tomographic retrieval setups, the size of the state and measurement space is rather large ( $n \approx 10^7$ ,  $m \approx 10^6$ ), and sparse matrix structures for storage and iterative methods for solving linear equation systems are applied. The typical memory and computing requirements for such a

setup are demanding and require the utilization of a parallel computer. The retrieval of the tomographic flight discussed in Sect. 5 was performed on six computing nodes with 48 CPU cores and 384 GB main memory.

## 4 ESSenCe

### 4.1 Overview

GLORIA was deployed during the ESSenCe campaign for the first time. The main objective of this campaign was the in-flight testing of the GLORIA instrument under stratospheric conditions and the first verification/validation of the GLORIA retrieval products (Kaufmann et al., 2013).

Most favorable conditions for such a test campaign are cloud-free conditions utilizing an aircraft carrier which can fly as high as possible into the stratosphere. For this purpose, the Russian M55 Geophysica was chosen, which has a ceiling altitude of about 21 km and a high probability to find mesoscale structures in the upper troposphere/lower stratosphere. The aircraft is highly flexible in terms of operations, and regarding ground weather and stratospheric conditions. The campaign base was Kiruna in northern Sweden.

The first part of the ESSenCe campaign consisted of ground-based measurements inside and outside of the hangar Arena Arctica to assure the interaction of all subsystems of the GLORIA instrument after transport and final integration. Several certification and calibration measurements were conducted, including electromagnetic tests of GLORIA when mounted on Geophysica.

The second part of the campaign consisted of flights with full instrumentation under stratospheric conditions. Flight patterns were planned such that the functionality and performance of GLORIA could be tested under all major conditions that are expected during later research flights. Particularly, this includes electromagnetic compatibility considerations (under flight conditions), the thermal behavior of the sensor and the gimbal frame, the detector and instrument optics cooling system, the pointing system, and the interferometer control system.

The dynamic conditions of the Arctic upper troposphere and lower stratosphere during the ESSenCe campaign were mostly undisturbed. At the beginning of the campaign in early December 2011, a low pressure system over the Norwegian Sea slowly approached Scandinavia. East of this low, mid-latitude air moved polewards, thereby being lifted isentropically. Connected to the low's frontal system, high clouds appeared south of this tongue of air (Fig. 1, blue lines). On the western rim of the low pressure system, air from the lower stratosphere descended deep into the troposphere, coiling up cyclonically. A few days later, the polar vortex strengthened and showed very low core temperatures with values well below 190 K in the lower stratosphere. Due to large-scale disturbances the vortex center moved towards

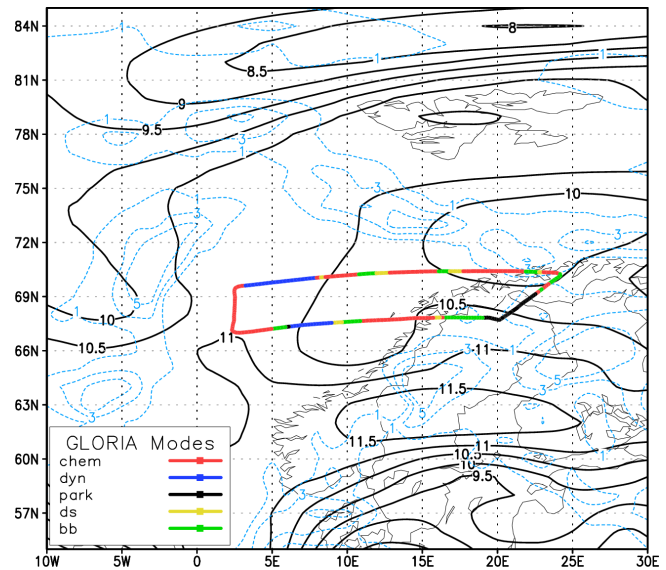


**Figure 1.** Potential vorticity (in PVU, black solid lines) on a 370 K isentropic surface (at approximately flight level) and cirrus clouds at lower levels (shown by cloud ice water content [ $10^5 \text{ kg kg}^{-1}$ ] on 280 K, blue lines) and the track of the Geophysica aircraft for ESSenCe flight 2 of 16 December 2011. The abbreviations “dyn” and “chem” mark dynamics- and chemistry-mode measurements of GLORIA, respectively; “park” indicates that GLORIA is in parking position; “ds” and “bb” indicate deep space and blackbody calibration measurements, respectively.

the European sector and air from the vortex edge moved polewards over Siberia, thus forming a broad intrusion of air with low potential vorticity reaching from Siberia across the North Pole to the Norwegian Sea.

### 4.2 GLORIA operations

Two GLORIA flights were performed during ESSenCe. Flight 1 took place on 11 December 2011, 11:00–15:00 UTC, and flight 2 on 16 December 2011, 14:00–17:50 UTC, respectively. Although the instrument encountered some technical problems, partly related to the extremely cold temperatures in the polar vortex, GLORIA took nominal atmospheric measurements including calibration for more than 1 h during each flight. During flight 1, all measurements were taken in chemistry mode while during flight 2, both chemistry and dynamics-mode measurements were performed.

Due to interferometer slide velocity variations during the first flight, these data were utilized for engineering purposes only. The functionality of the gimbal frame was partly lost in both flights after 1–2 h of flight time. For the remaining flight time it was not possible to further compensate the image rotation. The loss of pointing and image stabilization capabilities impacts data quality significantly such that Level 0 to Level 2 processing was restricted to the first measurement period of the second flight. The flight path of the Geophysica aircraft

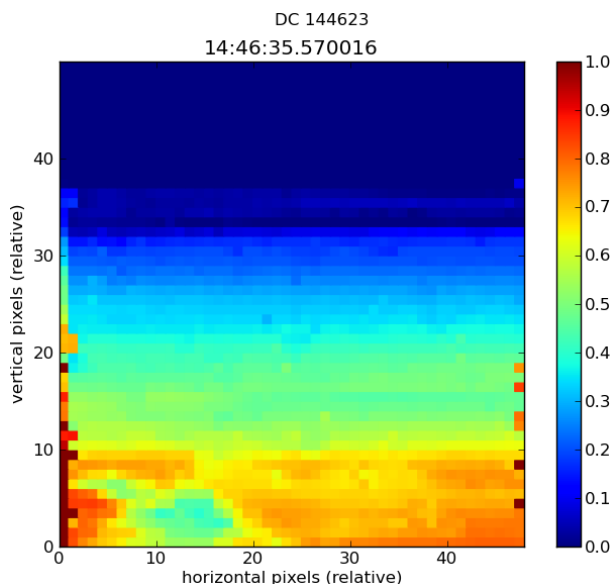


**Figure 2.** Direct current signal (arbitrary units) for one GLORIA image, before the Fourier transformation is applied. Exposure time is 40 ms and the horizontal extent is about 7.5 km at 10 km tangent altitude.

and GLORIA instrument operations during the second flight are illustrated in Fig. 1.

During both ESSenCe flights, one of the internal blackbodies and quasi-deep space spectra were used for two-point radiometric calibration. The latter exhibit remnants of atmospheric radiation, namely signatures of  $\text{CO}_2$  below  $750\text{ cm}^{-1}$ ,  $\text{O}_3$  around  $1050\text{ cm}^{-1}$ , and  $\text{CH}_4$  and  $\text{N}_2\text{O}$  around  $1300\text{ cm}^{-1}$ , which affect the radiometric accuracy. These spectral windows are not used in the retrieval.

A typical GLORIA raw data image is illustrated in Fig. 2. It demonstrates the ability of the instrument to resolve spatial structures in the atmosphere as low as 150 m in horizontal and vertical direction. Constantly high signals in the lower two-thirds of the image indicate gray body emissions from clouds or aerosol layers at these altitudes. In contrast to cloud sensing, the observation and quantification of trace gas filaments or temperature fluctuations does not require a horizontal resolution as provided by an individual GLORIA pixel. Although the Fourier transformation is initially applied to all individual detector pixels, only the mean value for each detector row is used in the subsequent Level 2 processing. No averaging in the vertical direction of the image is applied. This means that currently the information used is similar to that of a one-dimensional detector array, which registers a full spectrum in each pixel during an interferometer sweep.

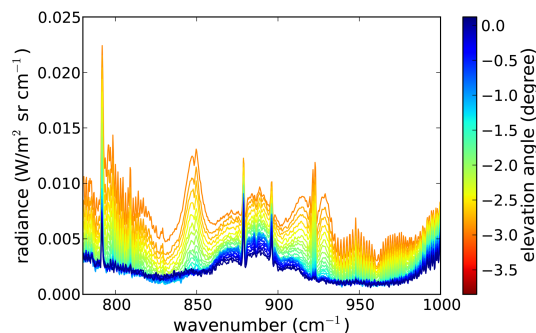


**Figure 3.** Spectra obtained by averaging over a detector row for a single GLORIA dynamics-mode measurement (Image 72, measured at 15:04:49 UTC at  $67^\circ\text{ N}$ ,  $7^\circ\text{ E}$ ) after pixel weighting and filtering. Corresponding tangent altitudes are 9 km (red) to 15 km (dark blue).

Before detector pixels are averaged in the horizontal domain, broken pixels (deviation of more than 2 times the standard deviation from the line average) or pixels pointing to clouds are removed. Entire detector rows are ignored if more than 75 % of the pixels are marked as broken or cloudy. Weighting of individual pixels is based on the noise analysis of blackbody spectra. Typical GLORIA dynamics-mode spectra for the binned data are illustrated in Fig. 3. The rovibrational emission lines of  $\text{CO}_2$  at  $792\text{ cm}^{-1}$ , CFC-11 at  $850\text{ cm}^{-1}$ , and  $\text{HNO}_3$  at  $890\text{ cm}^{-1}$  are clearly visible in the data.

Figure 4 illustrates the horizontal scan pattern of the GLORIA dynamics-mode measurements during ESSenCe. As stated above, the line of sight is panned from  $48$  to  $118^\circ$  with respect to the airplane nose. GLORIA dynamics-mode data were recorded from 14:58 to 15:10 UTC, yielding 121 individual images at about 2200 spectral points.

### 4.3 GLORIA Level 2 data analysis

#### 4.3.1 Retrieval Setup

The retrieval setup for GLORIA depends on the instrument performance and atmospheric conditions. It consists of the choice of spectral windows utilized for the radiative transfer forward model, the a priori and regularization parameters utilized in the constrained global fit method, and the error covariance matrix of the measurements.

The selection of appropriate spectral windows for the GLORIA dynamics-mode retrieval is non-trivial because the spectral resolution of this mode does not allow for the separation of individual trace gas emission lines. In addition, the radiometric calibration procedure utilizing “quasi-deep” space spectra (in contrast to “real deep” space spectra as observed from a satellite) causes a non-uniform error pattern in the wavelength domain. Therefore, the selection of spectral windows is performed by an automatic algorithm maximizing

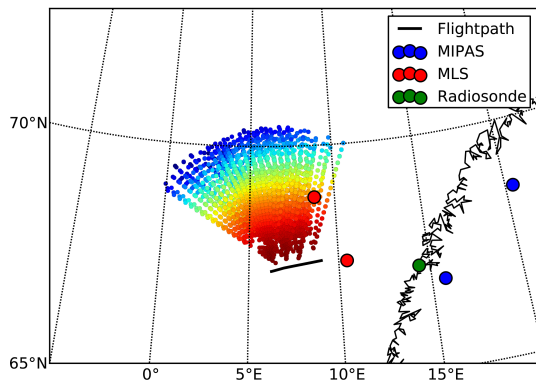


**Figure 4.** GLORIA tangent points of dynamics-mode measurements during ESSenCe flight 2. Tangent points closest (furthest) from the flight path (black line) are at highest (lowest) altitudes. Corresponding tangent altitudes are 4 km (red) to 15 km (blue). Thick, colored dots mark the geolocation of collocated MIPAS-Envisat and EOS-MLS tangent points and radiosonde positions. MIPAS-Envisat measurements were made on 16 December 2011 at 15:21 and 16:09 UTC, and EOS-MLS measurements at 11:40 and 11:42 UTC, respectively.

the information gain obtained by the measurements. The figure of merit for information gain is determined by the instrumental uncertainties and the a priori knowledge (Kullback and Leibler, 1951). This selection is performed by a newly developed genetic algorithm optimizing the spectral window size and position simultaneously (Blank, 2013). In contrast to previous work (von Clarmann and Echle, 1998; Dudhia et al., 2002), this method does not require pre-selected broader spectral ranges and is able to optimize several spectral windows simultaneously. The latter is most relevant here due to the limited spectral resolution of the GLORIA dynamics-mode measurements.

For ESSenCe, the main retrieval targets are temperature,  $O_3$ ,  $HNO_3$ , and CFC-12. The spectral windows as selected by the genetic algorithm to retrieve these quantities are illustrated in Fig. 5. There are twice as many spectral windows than main retrieval targets for considering cloud/aerosol effects as well as other contaminant gases. A priori data for the constrained global fit are taken from the MIPAS (Michelson Interferometer for Passive Atmospheric Sounding) reference atmospheres (Remedios et al., 2007). Some species (such as  $CO_2$ ) were updated to 2011 conditions. Pressure and temperature data were taken from the ECMWF ERA (European Centre for Medium-Range Weather Forecasts Re-Analysis)-Interim data set (Dee et al., 2011). The penalty of zero-order regularization (Eq. 2) was suppressed by a factor of 3 in comparison to an optimal estimation method assuming the standard deviations of the MIPAS climatology. For temperature and pressure, an uncertainty of 3 K and 1 % is assumed, respectively. Weighting factors for the first-order regularization in the vertical direction are inversely proportional to the standard deviations of the MIPAS climatology multiplied by

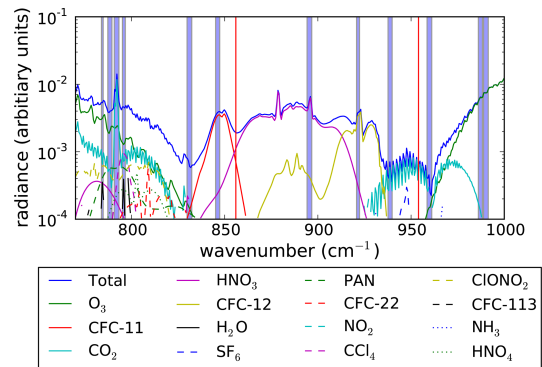


**Figure 5.** Simulated GLORIA dynamics-mode spectra for 16 km tangent altitude applying the MIPAS reference atmosphere for mid-latitudes. The spectral windows utilized in the retrieval are marked by blue vertical boxes.

a characteristic length scale of 0.25 km for temperature and CFC-12 and 1 km for  $O_3$  and  $HNO_3$ . The horizontal weighting factor is 100 km for all species.

The characterization of the GLORIA measurement error covariance matrix is a work in progress. The main source of uncertainty is instrument noise, approximated by a diagonal matrix assuming an uncertainty of  $25 \text{ nW}/(\text{cm}^2 \text{ cm}^{-1} \text{ sr})$  and 2 %, respectively. The transportation and mounting of the GLORIA instrument onto the aircraft, as well as thermal stress during a research flight may cause a misalignment between the GLORIA attitude control system and the interferometer's line of sight. Therefore, it is mandatory to verify the vertical pointing of the instrument and apply some corrections, if necessary. This is done by simulating the  $CO_2$  Q-branch emissions at  $792.5 \text{ cm}^{-1}$  adopting ECMWF temperature data for the entire flight. Assuming that the real atmosphere during a research flight has a mean temperature similar to ECMWF data, a single elevation angle correction is retrieved. In the case of ESSenCe flight 2 this correction is  $0.1955^\circ$ . Since the dominant uncertainties of the resulting line-of-sight elevation angles are not expected to change during the flight, small- and medium-scale structures in atmospheric temperature data can still be resolved by the measurement. The effect of the remaining pointing uncertainty of  $0.023^\circ$  is considered in the error budget of the retrieval targets (see Sect. 4.3.2).

#### 4.3.2 Results, uncertainties, and comparison to other measurements

Typical limb radiance altitude profiles for a few spectral windows are illustrated in Fig. 6. The intensities are generally increasing towards lower altitudes, as expected. The dynamical range given by maximum and minimum observed radiances in the considered spectral range varies between 50 and 500 % for tangent altitudes between 9 and 17 km, respectively.

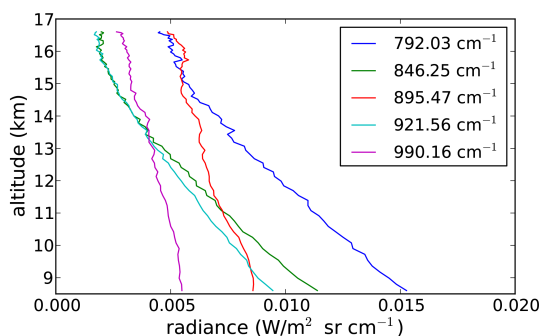


**Figure 6.** GLORIA integrated radiances for some spectral windows as selected by the genetic algorithm. The data is for Image 72 at 67° N and 7° E on 16 December, 15:05 UTC.

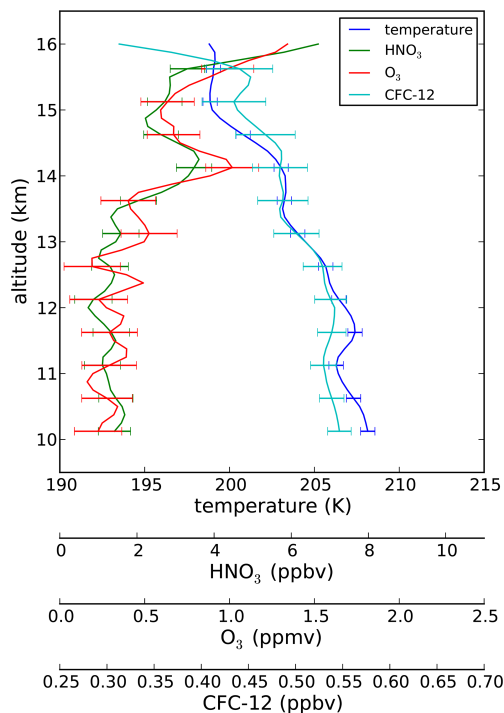


**Figure 7.** Retrieved temperature, HNO<sub>3</sub>, O<sub>3</sub>, and CFC-12 for GLORIA Image 72.

Corresponding retrieval results for the main targets of the GLORIA dynamics mode are illustrated in Fig. 7. The most prominent feature in the retrieved quantities is a pronounced enhancement of O<sub>3</sub> and HNO<sub>3</sub> around an altitude of 14 km, which may point to a filamentary structure in the stratosphere. This enhancement extends several hundred kilometers horizontally, as indicated by the two-dimensional cross-sections measured by GLORIA (Fig. 8). The uncertainties of HNO<sub>3</sub> and O<sub>3</sub> (Figs. 9–11) are on the order of 0.25 ppbv and 0.1 ppbv, respectively, and are dominated by detector noise. This means that the trace gas enhancement at 14 km is significant, whereas the small-scale structures below this altitude are within the noise error. The vertical resolution (Fig. 12)

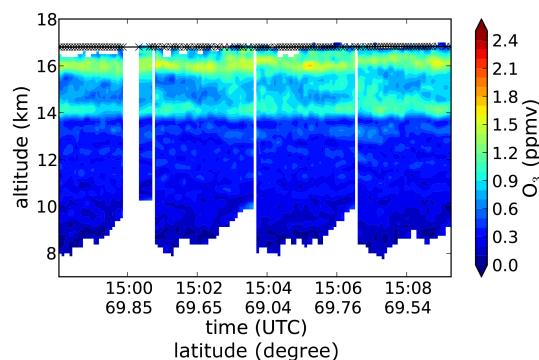


**Figure 8.** Retrieved ozone volume mixing ratio from GLORIA dynamics-mode data for 16 December 2011. Universal time and geographic latitude (in °) label the x axis. The figure shows four horizontal sweeps starting at 48° and ending at 118° with respect to the airplane nose.

is about 500 m for HNO<sub>3</sub> and O<sub>3</sub>, and somewhat worse for temperature (750 m) and CFC-12 (600–1400 m). The vertical gradient and (comparatively low) vertical resolution of CFC-12 dynamics-mode data do not allow for the resolution of the filament at 14 km, whereas the high vertical resolution of O<sub>3</sub> and HNO<sub>3</sub> should give a realistic picture of this structure.

To validate these GLORIA measurements the retrieved data are compared to several other instruments. These are the two limb emission sounders mounted on the same airplane as GLORIA, namely the MIPAS-STR (Michelson Interferometer for Passive Atmospheric Sounding – Stratospheric Aircraft) (Woiwode et al., 2012) and MARSCHALS (Millimetre-wave Airborne Receivers for Spectroscopic Characterization in Atmospheric Limb Sounding, Castelli et al., 2013) instruments. Furthermore, two in situ data sets obtained during the ascent and descent of the second ESSenCe flight are used for the comparison, namely measurements of the Whole Atmosphere Sampler (WAS; Laube et al., 2013) and the High Altitude Gas Analyzer (HAGAR; Volk et al., 2000; Werner et al., 2010) data sets. In addition, GLORIA measurements are compared to the satellite-borne limb emission measurements of MIPAS (Fischer et al., 2008) on ESA's Environmental Satellite (Envisat) and the Earth Observing System (EOS) Microwave Limb Sounder (EOS-MLS, data version v03.33; Froidevaux et al., 2008) on NASA's EOS AURA satellite. The MIPAS data were derived with the retrieval processor of the Karlsruhe Institute of Technology, data version V5R\_O3\_221 and V5R\_HNO3\_221 for ozone and HNO<sub>3</sub> (von Clarmann et al., 2009) and V5R\_CFC-11\_221 for CFC-11 (Kellmann et al., 2012). Finally, the GLORIA data are compared to simulations of the Chemical Lagrangian Model of the Stratosphere (CLaMS; Konopka et al., 2007; Grooß et al., 2014; Pommrich et al., 2014; Vogel et al., 2014, and references therein). CLaMS runs with full stratospheric chemistry (including heterogeneous chemistry and sedimentation) and

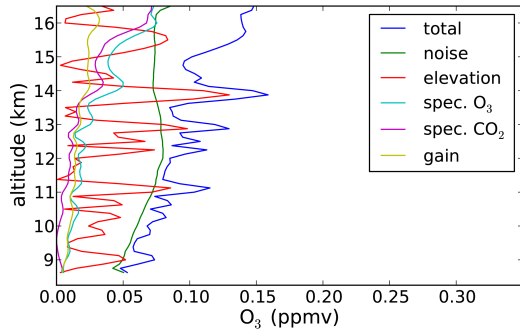


Figure 9. Error budget for O<sub>3</sub> for GLORIA Image 72.

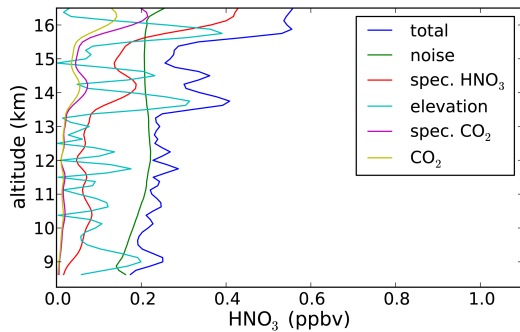


Figure 10. Error budget for HNO<sub>3</sub> for GLORIA Image 72.

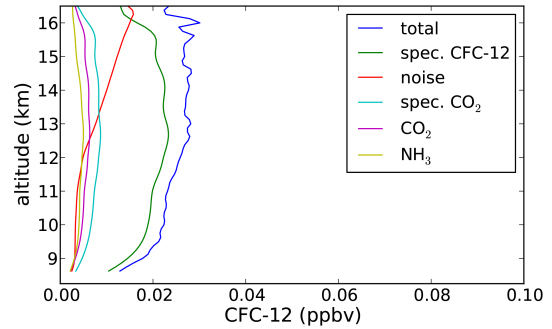


Figure 11. Error budget for CFC-12 for GLORIA Image 72.

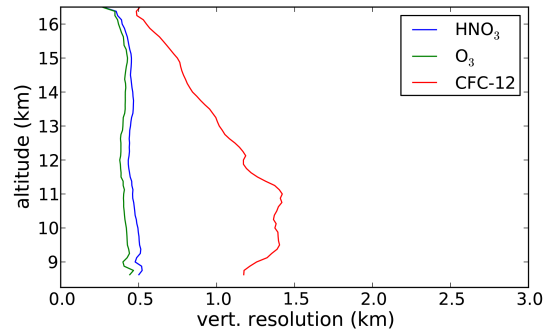


Figure 12. Vertical resolution for HNO<sub>3</sub>, O<sub>3</sub>, and CFC-12, for GLORIA Image 72.

is driven by ERA-Interim reanalysis data (for the detailed model setup, see Vogel et al., 2014). The simulations cover an altitude range from the surface up to the 900 K potential temperature with a horizontal resolution of approximately 100 km and a maximum vertical resolution of about 400 m around the tropopause. The simulations were initialized on 1 November 2011 (for ESSenCe) and on 1 May 2012 (for the TACTS/ESMVal campaign), respectively, using satellite measurements and tracer–tracer correlations following Grooß et al. (2014).

The mismatch in distance between the comparison data and GLORIA’s tangent points is typically a few hundred kilometers (Fig. 4). Since this is larger than the spatial extent of the GLORIA dynamics-mode measurements and since the atmospheric scene is relatively homogeneous in the horizontal direction (Fig. 8), the entire dynamics-mode sequence from 14:58 to 15:10 UTC was averaged for comparison with the other data sets. The error bars of an averaged profile is somewhat smaller than the uncertainties of an individual profile, but larger than the root mean squares error of the single errors of the set of profiles considered for an average.

The satellite instruments’ vertical profiles exhibit a much coarser altitude resolution than the GLORIA data. This effect is taken into account by convolving the GLORIA data  $\mathbf{x}_{\text{gloria}}$  with the averaging kernel of these instruments ( $A_{\text{mipas}}$  and  $A_{\text{mls}}$ ) considering the respective a priori data ( $\mathbf{x}_{\text{mipas}}^{\text{apr}}$  and

$\mathbf{x}_{\text{mls}}^{\text{apr}}$ ):

$$\mathbf{x}_{\text{gloria}}^{\text{conv}} = \mathbf{x}_{\text{mipas/mls}}^{\text{apr}} + A_{\text{mipas/mls}}(\mathbf{x}_{\text{gloria}} - \mathbf{x}_{\text{mipas/mls}}^{\text{apr}}). \quad (3)$$

Figures 13–15 show comparisons of GLORIA retrieval results with the different data sets described above. The left panels of these figures illustrate the data “as is”, and the right panel shows differences between GLORIA and the other data sets, where the effect of the averaging kernels was taken into account for the calculation of the differences. It is obvious that the effect of the averaging kernel is rather large for the comparison with the satellite instruments because the vertical resolution of the satellite data sets is several kilometers in the lower stratosphere.

GLORIA O<sub>3</sub> data show excellent agreement with MARSCHALS data, which were recorded a few minutes (14:52–14:56 UTC) before GLORIA dynamics-mode measurements. MARSCHALS O<sub>3</sub> abundance was retrieved from the Band B data (297–305 GHz). Differences between the two data sets are a few percent and smaller than the combined error bars. Most notable is the observation of the O<sub>3</sub> enhancement at 14 km in both data sets. Technical improvements of the MARSCHALS instrument and a new retrieval setup (Gerber, 2014) allowed the derivation of such a fine structure from MARSCHALS data for the first time. O<sub>3</sub> observations of MIPAS-STR exhibit similar absolute values, but the local enhancement at 14 km is not resolved due to the coarser alti-

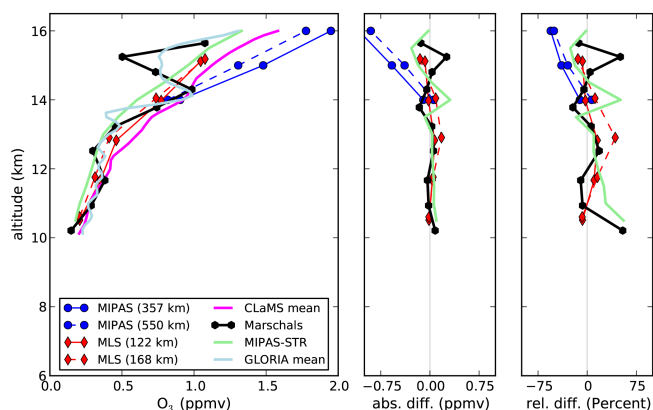


**Figure 13.** Comparison of  $O_3$  abundance between GLORIA dynamics-mode measurements and various collocated data sets.

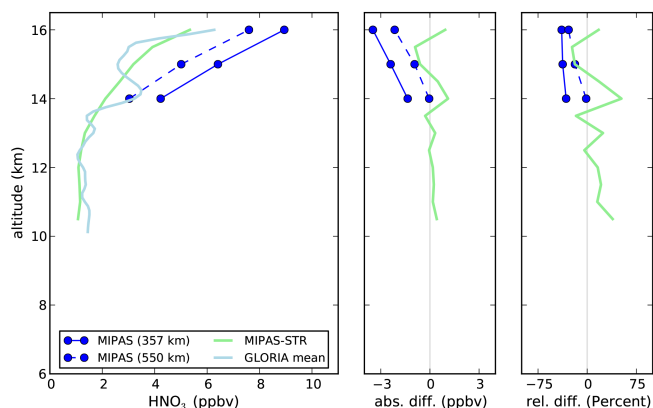


**Figure 14.** Comparison of  $HNO_3$  abundance between GLORIA dynamics-mode measurements and collocated data sets.

tude resolution of this data set. Differences to the satellite-borne data sets of EOS-MLS are typically less than 15 % and somewhat larger for MIPAS-Envisat, but both data sets cannot resolve the ozone enhancement at 14 km due to their broad averaging kernels. CLaMS model simulations do not show this localized enhancement either, which is consistent with the non-existence of this structure in the ERA-interim data at a resolution of  $1^\circ \times 1^\circ$  as utilized for this model run. However, modified potential vorticity data (Müller and Günther, 2003) based upon ECMWF operational analyses at a much higher spatial resolution ( $0.1^\circ \times 0.1^\circ$ , not shown here) reveals increased values at an altitude of 13.5 km at the location of the GLORIA measurements. This indicates that two different air masses moved close together, and model simulations at higher spatial resolution are needed to resolve such structures.

Mixing ratios of  $HNO_3$  measured from GLORIA and MIPAS-STR show similar values at most altitudes as well – differences are typically less than 15 %, except for the 14 km region, where GLORIA data is enhanced by more than 1 ppbv. MIPAS-Envisat  $HNO_3$  values (spatial separation

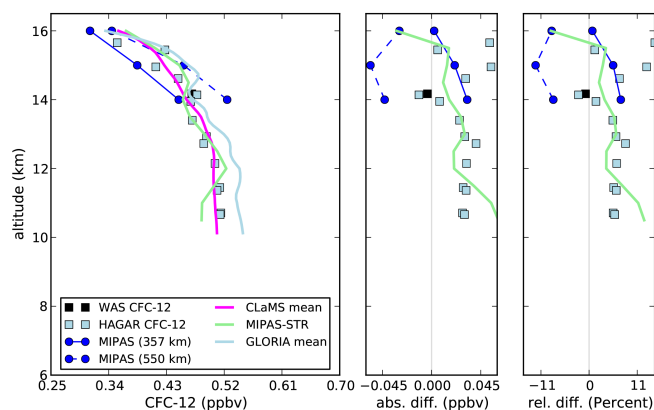


**Figure 15.** Comparison of CFC-12 abundance between GLORIA dynamics-mode measurements and collocated data sets.

350–550 km) are 20–50 % larger than the other two data sets, which may be due to the differences in the tangent point location and viewing geometry.

For CFC-12, GLORIA data shows a small high bias of about 5 % in the entire altitude region in comparison to collocated MIPAS-STR data. This bias is also observed in comparison to the CFC-12 data of the WAS and HAGAR in situ instruments measured during the ascent and descent of the aircraft. CLaMS results are in good agreement with the in situ measurements. Although this difference between GLORIA and the in situ or model data is within the error margins of the GLORIA instrument, it may point to some instrumental issues to be solved in future missions.

## 5 The TACTS/ESMVal Campaign

### 5.1 Overview

The second deployment of GLORIA was during the TACTS/ESMVal campaign in September 2012. This campaign was conducted by means of the new German High Altitude and Long Range Research Aircraft. It covered a broad geographical region from Spitsbergen at high northern latitudes to Antarctica in the south and from western Africa in the west to the Arabian Sea in the east. The main scientific objective of the TACTS campaign is the measurement of the composition of the lowermost stratosphere during the period from summer to autumn to quantify the transport and mixing in the upper troposphere/lower stratosphere in the vicinity of the subtropical jet. The ESMVal campaign aimed to provide a large set of constituent, aerosol, and cloud data for the validation and improvement of chemistry–climate models. TACTS/ESMVal yielded nearly 90 h of GLORIA measurements at different atmospheric conditions and measurement modes.

The aim of this section is to show some preliminary results regarding the three-dimensional reconstruction of a fil-

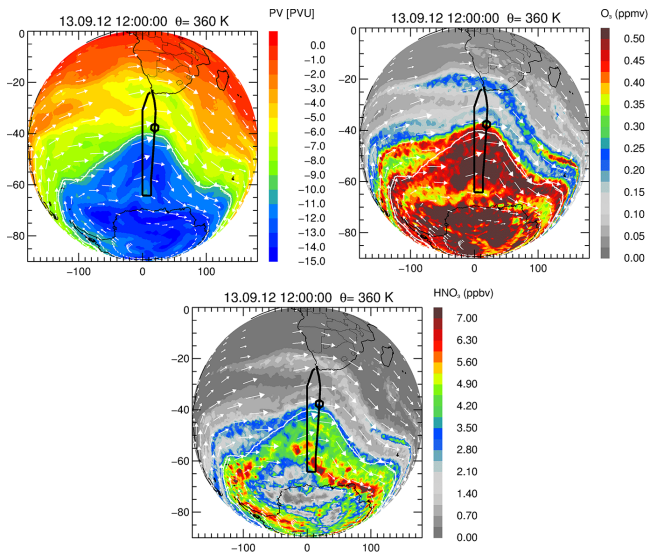


**Figure 16.** ECMWF potential vorticity (left) at a potential temperature of 360 K (about 12 km altitude) for the TACTS/ESMVal flight on 13 September 2012. The flight track is indicated by a black line. At 45° S, 20° E a tomographic flight pattern (approximate altitude of about 12.5 km) was performed. The lower and right-hand plots show O<sub>3</sub> and HNO<sub>3</sub> volume mixing ratios at 360 K as simulated by the CLaMS model, respectively. The vortex edge is calculated as defined by Nash et al. (1996) and is marked by a white contour line. The horizontal winds are indicated by white arrows.

ament, thereby demonstrating the outstanding capabilities of GLORIA to resolve such small-scale structures in all three dimensions.

## 5.2 GLORIA measurements

Since implementation during ESSenCe, the GLORIA instrument was subject to several improvements. Problems with the gimbal frame and with some interferometer components have been solved, and instrument configurations have been optimized. The spectral resolution of the dynamics mode during TACTS/ESMVal has been reduced by a factor of two compared to ESSenCe.

During TACTS/ESMVal, the aircraft flew on several closed loop flight tracks to test GLORIA's capabilities to sound the atmosphere tomographically. One of these closed flight path tracks took place on 13 September 2012 south of Africa at the edge of the Antarctic polar vortex (Fig. 16). This region is characterized by strong gradients of potential vorticity, ozone, and HNO<sub>3</sub> mixing ratios. At the edge of the polar vortex, HALO performed a hexagonal flight track such that the GLORIA lines of sight are directed to the center of the hexagon. At this location (45° S, 20° E) the horizontal winds are sheared and tilted as a consequence of a distortion of the jet stream at lower altitudes (Fig. 17). Wind speeds are on the order of 45 m s<sup>-1</sup>.

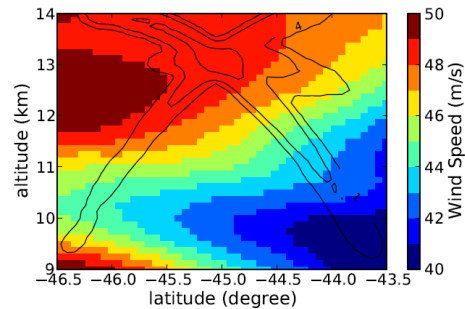


**Figure 17.** Horizontal wind speeds at 20° E for 13 September 2012, 14:00 UTC. Contour lines indicate the number of tangent points per grid cell. The outer (middle, inner) line marks 2 (4, 16) points/cell.

To retrieve the atmospheric composition within the air volume contained by the hexagon, an appropriate atmospheric grid was defined. The size of the grid cells is based on the vertical and horizontal field of view of the GLORIA instrument, namely 125 m in the vertical and 7.5 km in the horizontal direction, respectively, resulting in about  $2 \times 10^6$  individual cells. The size of the grid cells increases towards the boundaries of the air volume.

The horizontal and vertical regularization applied to the retrieval targets is similar to that in ESSenCe, as is the selection of spectral windows. The reduced spectral resolution and uncertainties in the instrument calibration led to the elimination of a few spectral windows describing the aerosol background and some “secondary” gases such as PAN or ClONO<sub>2</sub>, which cannot be retrieved with high confidence for these atmospheric conditions. The most relevant difference to ESSenCe is the omission of the spectral window at 845 cm<sup>-1</sup> showing strong CFC-11 emissions, which turned out to be contaminated by instrument emissions from the optical window of GLORIA (Kleinert et al., 2014). Cloud indices (Spang et al., 2004) observed during the hexagonal flight were 4–6 between 9 and 14 km, indicating an almost cloud-free atmosphere.

Retrieved temperature and constituent fields exhibit a pronounced intrusion of stratospheric air into the troposphere at about 45° S, 20° E (Figs. 18 and 19). This intrusion is observed between an altitude of 12.5 and 14.5 km and extends about 500 m vertically. The horizontal extent is at least 200 km. Its stratospheric nature is indicated by enhanced HNO<sub>3</sub> and O<sub>3</sub> – at least by a factor of 2 compared to the air parcels just below or above the filament. This enhancement is significantly larger than the uncertainty of these species. Temperature data do not show this filamentary structure and varies by less than 2 K in the vicinity of this structure – in accordance with our expectation that this intrusion is caused by chaotic advection and not by adiabatic movements. It should be noted that CFC-12 does not show a pronounced structure due to its weak vertical gradient at these altitudes.

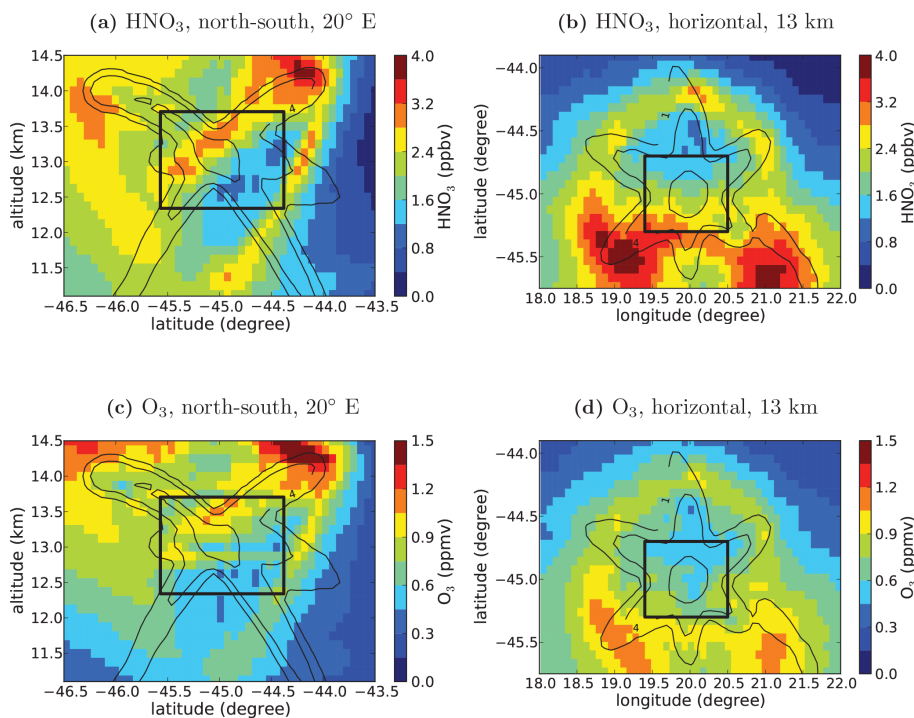


**Figure 18.** Retrieved  $\text{HNO}_3$  and  $\text{O}_3$  mixing ratios at  $20^\circ\text{E}$  (left) and 13 km altitude (right) for 13:30–14:30 UTC, 13 September 2012. For details see caption of Fig. 17.

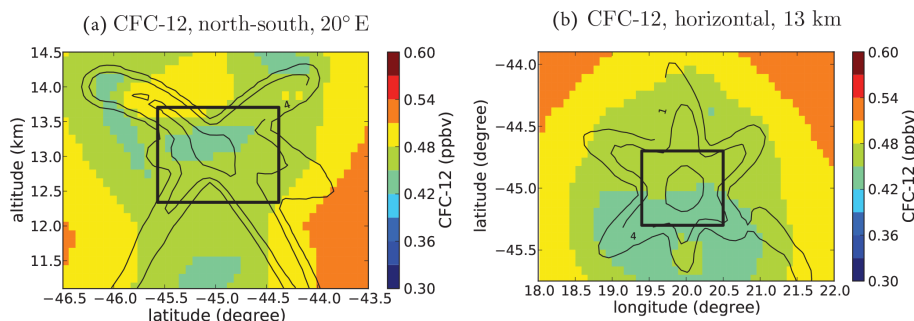


**Figure 19.** Retrieved CFC-12 mixing ratios at  $20^\circ\text{E}$  (left) and 13 km altitude (right) for 13:30–14:30 UTC, 13 September 2012. For details see caption of Fig. 17.

Using three-dimensional tomography, the horizontal resolution is up to 20 km in the core of the measured atmospheric region (Fig. 20). In this region, each atmospheric grid cell is measured from at least four different directions. The vertical resolution of the atmospheric fields is 200–300 m and somewhat larger than for the data obtained from the linear flight tracks during ESSenCe due to the increased instrument performance of GLORIA during the TACTS/ESMVal campaign. Since the calculation of retrieval diagnostics such as averaging kernel and spatial resolution is computationally very demanding (it breaks the sparsity of the computational problem; see, e.g., Ungermann et al., 2010), this information

has not been calculated for all atmospheric grids cells considered in the retrieval. Although the horizontal wind speed is rather large in the vicinity of the GLORIA measurements, the alignment of the filamentary structure with respect to the dominant wind direction does not expect to smear out the gradients significantly. However, future data versions will consider the effect of advection in the tomographic reconstruction of small-scale structures.

A preliminary comparison to the CLaMS simulation for this flight (Fig. 16) indicates that the model resolution of 100 km (horizontally) is in turn not sufficient to resolve this intrusion of air as observed by the tomographic sounding.

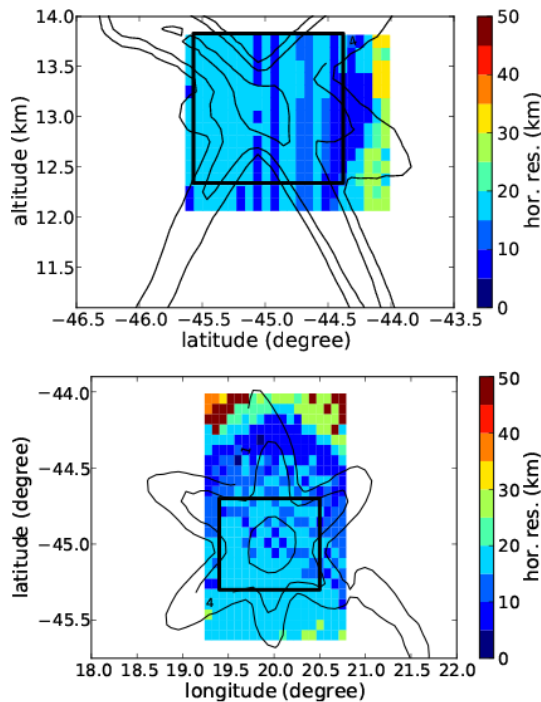


**Figure 20.**  $\text{HNO}_3$  horizontal resolution at  $20^\circ$  E (top) and 13 km altitude (bottom). For details see caption of Fig. 17.

### 5.3 Advantages of Tomographic Sounding

The major improvement of three-dimensional limb sounding compared to conventional limb sounding not applying tomographic inversion techniques is the reduction of the horizontal (line-of-sight) smearing of these instruments. This is particularly important if the small-scale structure to be observed is smaller than the horizontal averaging kernel or if it is not co-aligned with the instrument's line of sight. Figure 21 illustrates this effect in the case of the filament observed during TACTS/ESMVal. The plot on the right hand side shows the three-dimensional reconstruction of the  $\text{HNO}_3$  filament (Fig. 18), sampled at the tangent points of each segment of the hexagon. The plot on the left hand side shows the result of a conventional one-dimensional retrieval approach assuming horizontal homogeneity along the instrument's line of sight. The quality of the match between the retrieved structures and the tilt of the filament is dependent on a good alignment of the line of sight of a given segment and that of the filament. An example of a good match is found at 13:50; whereas a worse case is found at 13:40 UTC. Since the orientation of the filament is generally not known a priori, the tomographic data gives a more realistic picture of the structure.

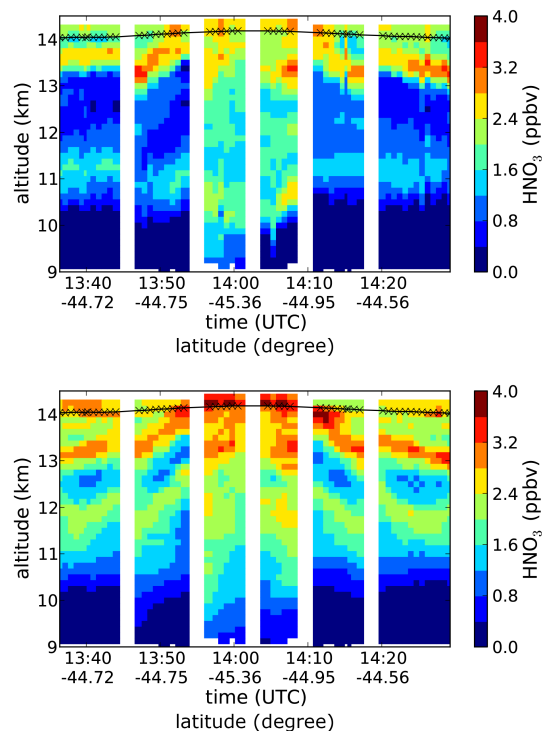


**Figure 21.** Comparison between a one-dimensional (top) and three-dimensional (bottom) reconstruction of  $\text{HNO}_3$  during the GLORIA hexagonal flight. The segments of the hexagon are separated by white stripes. Measurement time (UTC) and latitude (degree) for the beginning of each segment are given on the  $x$  axis.

## 6 Conclusions

The first two deployments of GLORIA demonstrated the readiness of this instrument to measure upper-tropospheric/lower-stratospheric composition at high spatial resolution. The retrieval of temperature,  $\text{O}_3$ ,  $\text{HNO}_3$ , and CFC-12 presented no major problems except for a small bias in CFC-12 data. Increased effort in the radiometric calibration procedure will reduce this bias in future data versions. During ESSenCe, GLORIA already demonstrated its ability to measure intrusions of stratospheric air on vertical scales as low as a few hundred meters. However, the outstanding capability of the GLORIA instrument can only reach its full potential when the carrying aircraft flies a closed path around the air volume to be observed as performed several times during the TACTS/ESMVal campaign. In these cases, GLORIA data can provide three-dimensional constituent data at horizontal scales as low as a few tens of kilometers.

GLORIA represents the first airborne realization of the infrared limb imaging technique. The capabilities of this technique were also studied for application from a satellite in low Earth orbit (ESA, 2012). Although the observational mode of the satellite instrument is somewhat different from the airborne version, trace gas fields can be obtained with a similar

horizontal resolution as for the tomographic reconstruction of airborne GLORIA dynamics-mode data as presented in this study.

**Acknowledgements.** We acknowledge financial support by the German Helmholtz society (ATMO, ATMONSYS), by the European Space Agency/Mission Science Division (ESSENce), and the Deutsche Forschungsgemeinschaft in the priority program 1294 Atmospheric and Earth system research with the High Altitude and Long Range Research Aircraft (HALO). GLORIA retrieval activities were supported under the DFG project RASGLO (HALO-SPP 1294/Ka 2324/1-2) and flight planning by CLaMS model forecasts under the DFG project LASSO (HALO-SPP 1294/GR 3786).

We thank all members of the GLORIA instrument team for their extensive efforts in the development of the GLORIA instrument and the undertaking of the ESSENce and TACTS/ESMVal campaigns.

We acknowledge the contribution of L. Hoffmann and S. Griessbach (both at Research Center Jülich), G. Geppert (now at Max Planck Institute for Meteorology), Ch. Kaliczinsky (Wuppertal University), and K. Leppkes and J. Lotz (both at RWTH Aachen) for their contribution to the development of the retrieval code.

We would like to thank Th. Roeckmann (Institute for Marine and Atmospheric Research Utrecht, Utrecht University) and J. Laube (School of Environmental Sciences, University of East Anglia) for providing the Whole Atmosphere Sampler data.

We thank J. Wintel (Physics Department, University of Wuppertal) for the measurement of the High Altitude Gas Analyzer data.

We thank the satellite group at IMK-ASF for providing the MIPAS data, the MLS team for providing EOS-MLS data, and the CLaMS team for assistance in flight planning.

Finally, we would like to acknowledge the open source community for the development of programming and visualization tools such as scientific python, matplotlib, and swig.

The service charges for this open access publication have been covered by a Research Centre of the Helmholtz Association.

Edited by: J. Notholt

## References

- Blank, J.: Tomographic retrieval of atmospheric trace gases observed by GLORIA, Ph. D. thesis, Bergische Universität Wuppertal, 2013.
- Castelli, E., M. Dinelli, B., Del Bianco, S., Gerber, D., Moyna, B. P., Siddans, R., Kerridge, B. J., and Cortesi, U.: Measurement of the Arctic UTLS composition in presence of clouds using millimetre-wave heterodyne spectroscopy, *Atmos. Meas. Tech.*, 6, 2683–2701, doi:10.5194/amt-6-2683-2013, 2013.
- Curtis, A. R.: Discussion of “A statistical model for water vapour absorption” by R. M. Goody, *Quart. J. Roy. Meteorol. Soc.*, 78, 638–640, 1952.
- Dee, D. P., Uppala, S. M., Simmons, A. J., Berrisford, P., Poli, P., Kobayashi, S., Andrae, U., Balmaseda, M. A., Balsamo, G., Bauer, P., Bechtold, P., Beljaars, A. C. M., van de Berg, L., Bidlot, J., Bormann, N., Delsol, C., Dragani, R., Fuentes, M., Geer, A. J., Haimberger, L., Healy, S. B., Hersbach, H., Hólm, E. V., Isaksen, I., Kållberg, P., Köhler, M., Matricardi, M., McNally, A. P., Monge-Sanz, B. M., Morcrette, J.-J., Park, B.-K., Peubey, C., de Rosnay, P., Tavolato, C., Thépaut, J.-N. and Vitart, F.: The ERA-Interim reanalysis: configuration and performance of the data assimilation system, *Q. J. R. Meteorol. Soc.*, 137, 553–597, doi:10.1002/qj.828, 2011.
- Dudhia, A.: Michelson Interferometer for Passive Atmospheric Sounding (MIPAS) Reference Forward Model (RFM), Software Users Manual, available at: <http://eodg.atm.ox.ac.uk/RFM/sum/> (last access: December 2014), 2000.
- Dudhia, A., Jay, V. L., and Rodgers, C. D.: Microwindow Selection for High-Spectral-Resolution Sounders, *Appl. Opt.*, 41, 3665–3673, doi:10.1364/AO.41.003665, 2002.
- ESA: Report for Mission Selection: PREMIER, vol. SP-1324/3, ESA Communication Production Office, Noordwijk, the Netherlands, 2012.
- Fischer, H., Birk, M., Blom, C., Carli, B., Carlotti, M., von Clarman, T., Delbouille, L., Dudhia, A., Ehrt, D., Endemann, M., Flaud, J. M., Gessner, R., Kleinert, A., Koopman, R., Langen, J., López-Puertas, M., Mosner, P., Nett, H., Oelhaf, H., Perron, G., Remedios, J., Ridolfi, M., Stiller, G., and Zander, R.: MIPAS: an instrument for atmospheric and climate research, *Atmos. Chem. Phys.*, 8, 2151–2188, doi:10.5194/acp-8-2151-2008, 2008.
- Francis, G. L., Edwards, D. P., Lambert, A., Halvorson, C. M., Lee-Taylor, J. M., and Gille, J. C.: Forward modeling and radiative transfer for the NASA EOS-Aura High Resolution Dynamics Limb Sounder (HIRDLS) instrument, *J. Geophys. Res.-Atmos.*, 111, D13301, doi:10.1029/2005JD006270, 2006.
- Friedl-Vallon, F., Gulde, T., Hase, F., Kleinert, A., Kulesa, T., Maucher, G., Neubert, T., Olschewski, F., Piesch, C., Preusse, P., Rongen, H., Sartorius, C., Schneider, H., Schönfeld, A., Tan, V., Bayer, N., Blank, J., Dapp, R., Ebersoldt, A., Fischer, H., Graf, F., Guggenmoser, T., Höpfner, M., Kaufmann, M., Kretschmer, E., Latzko, T., Nordmeyer, H., Oelhaf, H., Orphal, J., Riese, M., Schardt, G., Schillings, J., Sha, M. K., Suminska-Ebersoldt, O., and Ungermann, J.: Instrument concept of the imaging Fourier transform spectrometer GLORIA, *Atmos. Meas. Tech.*, 7, 3565–3577, doi:10.5194/amt-7-3565-2014, 2014.
- Froidevaux, L., Jiang, Y. B., Lambert, A., Livesey, N. J., Read, W. G., Waters, J. W., Browell, E. V., Hair, J. W., Avery, M. A., McGee, T. J., Twigg, L. W., Sunmicht, G. K., Jucks, K. W., Margitan, J. J., Sen, B., Stachnik, R. A., Toon, G. C., Bernath, P. F., Boone, C. D., Walker, K. A., Filipiak, M. J., Harwood, R. S., Fuller, R. A., Manney, G. L., Schwartz, M. J., Daffer, W. H., Drouin, B. J., Cofield, R. E., Cuddy, D. T., Jarnot, R. F., Knosp, B. W., Perun, V. S., Snyder, W. V., Stek, P. C., Thurstans, R. P., and Wagner, P. A.: Validation of Aura Microwave Limb Sounder stratospheric ozone measurements, *J. Geophys. Res.-Atmos.*, 113, doi:10.1029/2007JD008771, 2008.
- Gerber, D.: RAL algorithm for retrievals of vertical trace gas profiles from the ESA UTLS limb sounder MARSCHALS, *Atmos. Meas. Tech. Discuss.*, in preparation, 2014.
- Gettelman, A., Hoor, P., Pan, L. L., Randel, W. J., Heglin, M. I., and Birner, T.: The Extratropical Upper Troposphere And Lower Stratosphere, *Rev. Geophys.*, 49, RG3003, doi:10.1029/2011RG000355, 2011.

- Godson, W. L.: The evaluation of infra-red radiative fluxes due to atmospheric water vapour, *Quart. J. Roy. Meteorol. Soc.*, 79, 367–379, 1953.
- Gordley, L. L. and Russell, J. M.: Rapid inversion of limb radiance data using an emissivity growth approximation, *Appl. Optics*, 20, 807–813, doi:10.1364/AO.20.000807, 1981.
- Groß, J.-U., Engel, I., Borrmann, S., Frey, W., Günther, G., Hoyle, C. R., Kivi, R., Luo, B. P., Molleker, S., Peter, T., Pitts, M. C., Schlager, H., Stiller, G., Vömel, H., Walker, K. A., and Müller, R.: Nitric acid trihydrate nucleation and denitrification in the Arctic stratosphere, *Atmos. Chem. Phys.*, 14, 1055–1073, doi:10.5194/acp-14-1055-2014, 2014.
- Hoor, P., Fischer, H., Lange, L., Lelieveld, J., and Brunner, D.: Seasonal variations of a mixing layer in the lowermost stratosphere as identified by the CO-O3 correlation from in situ measurements, *J. Geophys. Res.-Atmos.*, 107, 4044, doi:10.1029/2000JD000289, 2002.
- Kaufmann, M., Blank, J., Friedl-Vallon, F., Gerber, D., Guggenmoser, T., Höpfner, M., Kleinert, A., Sha, M. K., Oelhaf, H., Riese, M., Suminska-Ebersoldt, O., Woiwode, W., Siddans, R., Kerridge, B., Moyna, B., Rea, S., and Oldfield, M.: Technical Assistance for the Deployment of Airborne Limbsounders during ESSenCe, Tech. rep., European Space Agency, 2013.
- Kellmann, S., von Clarmann, T., Stiller, G. P., Eckert, E., Glatthor, N., Höpfner, M., Kiefer, M., Orphal, J., Funke, B., Grabowski, U., Linden, A., Dutton, G. S., and Elkins, J. W.: Global CFC011 (CCl<sub>3</sub>F) and CFC-12 (CCl<sub>2</sub>F<sub>2</sub>) measurements with the Michelson Interferometer for Passive Atmospheric Sounding (MIPAS): retrieval, climatologies and trends, *Atmos. Chem. Phys.*, 12, 11857–11875, doi:10.5194/acp-12-11857-2012, 2012.
- Kleinert, A., Friedl-Vallon, F., Guggenmoser, T., Höpfner, M., Neubert, T., Ribalda, R., Sha, M. K., Ungermann, J., Blank, J., Ebersoldt, A., Kretschmer, E., Latzko, T., Oelhaf, H., Olschewski, F., and Preusse, P.: Level 0 to 1 processing of the imaging Fourier transform spectrometer GLORIA: generation of radiometrically and spectrally calibrated spectra, *Atmos. Meas. Tech. Discuss.*, 7, 2827–2878, doi:10.5194/amtd-7-2827-2014, 2014.
- Konopka, P., Günther, G., Müller, R., dos Santos, F. H. S., Schiller, C., Ravegnani, F., Ulanovsky, A., Schlager, H., Volk, C. M., Viciani, S., Pan, L. L., McKenna, D.-S., and Riese, M.: Contribution of mixing to upward transport across the tropical tropopause layer (TTL), *Atmos. Chem. Phys.*, 7, 3285–3308, doi:10.5194/acp-7-3285-2007, 2007.
- Kullback, S. and Leibler, R. A.: On Information and Sufficiency, *The Annals of Mathematical Statistics*, 22, 79–86, doi:10.1214/aoms/1177729694, 1951.
- Laube, J. C., Keil, A., Bönisch, H., Engel, A., Röckmann, T., Volk, C. M., and Sturges, W. T.: Observation-based assessment of stratospheric fractional release, lifetimes, and ozone depletion potentials of ten important source gases, *Atmos. Chem. Phys.*, 13, 2779–2791, doi:10.5194/acp-13-2779-2013, 2013.
- Lotz, J., Naumann, U., and Ungermann, J.: Efficient Discrete Adjoint Computation in a Spectral Simulation Code, Tech. Rep. AIB-2011-05, RWTH Aachen and Forschungszentrum Jülich, 2011.
- Manney, G. L., Hegglin, M. I., Daffer, W. H., Santee, M. L., Ray, E. A., Pawson, S., Schwartz, M. J., Boone, C. D., Froidevaux, L., Livesey, N. J., Read, W. G., and Walker, K. A.: Jet characterization in the upper troposphere/lower stratosphere (UTLS): applications to climatology and transport studies, *Atmos. Chem. Phys.*, 11, 6115–6137, doi:10.5194/acp-11-6115-2011, 2011.
- Marshall, B. T., Gordley, L. L., and Chu, D. A.: BANDPAK: Algorithms for modeling broadband transmission and radiance, *J. Quant. Spectrosc. Ra.*, 52, 581–599, doi:10.1016/0022-4073(94)90026-4, 1994.
- Müller, R. and Günther, G.: A generalized form of Lait's modified potential vorticity, *J. Atmos. Sci.*, 60, 2229–2237, 2003.
- Nash, E. R., Newman, P. A., Rosenfield, J. E., and Schoeberl, M. R.: An objective determination of the polar vortex using Ertel's potential vorticity, *J. Geophys. Res.*, 101, 9471–9478, 1996.
- Olschewski, F., Ebersoldt, A., Friedl-Vallon, F., Gutschwager, B., Hollandt, J., Kleinert, A., Monte, C., Piesch, C., Preusse, P., Rolf, C., Steffens, P., and Koppmann, R.: The in-flight blackbody calibration system for the GLORIA interferometer on board an airborne research platform, *Atmos. Meas. Tech.*, 6, 3067–3082, doi:10.5194/amt-6-3067-2013, 2013.
- Olsen, M. A., Douglass, A. R., Newman, P. A., Gille, J. C., Nardi, B., Yudin, V. A., Kinnison, D. E., and Khosravi, R.: HIRDLS observations and simulation of a lower stratospheric intrusion of tropical air to high latitudes, *Geophys. Res. Lett.*, 35, L21813, doi:10.1029/2008GL035514, 2008.
- Piesch, C., Gulde, T., Sartorius, C., Friedl-Vallon, F., Seefeldner, M., Wölfel, M., Blom, C., and Fischer, H.: Design of a MIPAS instrument for high-altitude aircraft, in: Second International Airborne Remote Sensing Conference and Exhibition, 24, 27 p., 1996.
- Pommrich, R., Müller, R., Groß, J.-U., Konopka, P., Ploeger, F., Vogel, B., Tao, M., Hoppe, C. M., Günther, G., Spelten, N., Hoffmann, L., Pumphrey, H.-C., Viciani, S., D'Amato, F., Volk, C. M., Hoor, P., Schlager, H., and Riese, M.: Tropical troposphere to stratosphere transport of carbon monoxide and long-lived trace species in the Chemical Lagrangian Model of the Stratosphere (CLaMS), *Geosci. Model Dev.*, 7, 2895–2916, doi:10.5194/gmd-7-2895-2014, 2014.
- Remedios, J. J., Leigh, R. J., Waterfall, A. M., Moore, D. P., Sembhi, H., Parkes, I., Greenhough, J., Chipperfield, M.P., and Hauglustaine, D.: MIPAS reference atmospheres and comparisons to V4.61/V4.62 MIPAS level 2 geophysical data sets, *Atmos. Chem. Phys. Discuss.*, 7, 9973–10017, doi:10.5194/acpd-7-9973-2007, 2007.
- Riese, M., Preusse, P., Spang, R., Ern, M., Jarisch, M., Grossmann, U., and Offermann, D.: Measurements of trace gases by the CRYogenic Infrared Spectrometers and Telescopes for the Atmosphere (CRISTA) experiment, *Adv. Space Res.*, 19, 563–566, doi:10.1016/S0273-1177(97)00172-5, 1997.
- Riese, M., Tie, X., Brasseur, G., and Offermann, D.: Three-dimensional simulation of stratospheric trace gas distributions measured by CRISTA, *J. Geophys. Res.-Atmos.*, 104, 16419–16435, doi:10.1029/1999JD900178, 1999.
- Riese, M., Ploeger, F., Rap, A., Vogel, B., Konopka, P., Dameris, M., and Forster, P.: Impact of uncertainties in atmospheric mixing on simulated UTLS composition and related radiative effects, *J. Geophys. Res.*, 117, D16305, doi:10.1029/2012JD017751, 2012.
- Riese, M., Oelhaf, H., Preusse, P., Blank, J., Ern, M., Friedl-Vallon, F., Fischer, H., Guggenmoser, T., Höpfner, M., Hoor, P., Kaufmann, M., Orphal, J., Plöger, F., Spang, R., Suminska-Ebersoldt, O., Ungermann, J., Vogel, B., and Woiwode, W.: Gimballing Limb Observer for Radiance Imaging of the Atmosphere (GLO-

- RIA) scientific objectives, *Atmos. Meas. Tech.*, 7, 1915–1928, doi:10.5194/amt-7-1915-2014, 2014.
- Rothman, L., Gordon, I., Babikov, Y., Barbe, A., Benner, D. C., Bernath, P., Birk, M., Bizzocchi, L., Boudon, V., Brown, L., Campargue, A., Chance, K., Cohen, E., Coudert, L., Devi, V., Drouin, B., Fayt, A., Flaud, J.-M., Gamache, R., Harrison, J., Hartmann, J.-M., Hill, C., Hodges, J., Jacquemart, D., Jolly, A., Lamouroux, J., Roy, R. L., Li, G., Long, D., Lyulin, O., Mackie, C., Massie, S., Mikhailenko, S., Müller, H., Naumenko, O., Nikitin, A., Orphal, J., Perevalov, V., Perrin, A., Polovtseva, E., Richard, C., Smith, M., Starikova, E., Sung, K., Tashkun, S., Tennyson, J., Toon, G., Tyuterev, V., and Wagner, G.: The HITRAN2012 molecular spectroscopic database, *J. Quant. Spectrosc. Ra.*, 130, 4–50, doi:10.1016/j.jqsrt.2013.07.002, 2013.
- Seo, K.-H. and Bowman, K. P.: Lagrangian estimate of global stratosphere-troposphere mass exchange, *J. Geophys. Res.: Atmos.*, 107, ACL 2-1–ACL 2-8, doi:10.1029/2002JD002441, 2002.
- Solomon, S., Qin, D., Manning, M., Alley, R., Berntsen, T., Bindoff, N., Chen, Z., Chidthaisong, A., Gregory, J., Hegerl, G., Heimann, M., Hewitson, B., Hoskins, B., Joos, F., Jouzel, J., Kattsov, V., Lohmann, U., Matsuno, T., Molina, M., Nicholls, N., J.Overpeck, Raga, G., Ramaswamy, V., Ren, J., Rusticucci, M., Somerville, R., Stocker, T., Whetton, P., Wood, R. A., and Wratt, D.: *Climate Change 2007 – The Physical Science Basis. Contribution of Working Group I to the Fourth Assessment Report of the Intergovernmental Panel on Climate Change, Technical Summary*, Cambridge University Press, Cambridge, UK and New York, USA, 19–91, 2007.
- Spang, R., Remedios, J. J., and Barkley, M. P.: Colour indices for the detection and differentiation of cloud type in infrared limb emission spectra, *Adv. Space Res.*, 33, 1041–1047, doi:10.1016/S0273-1177(03)00585-4, 2004.
- Twomey, S.: *Introduction to the Mathematics of Inversion in Remote Sensing and Indirect Measurements*, Dover Publications, Mineola, N.Y. 11501, USA, 1977.
- Ungermann, J., Kaufmann, M., Hoffmann, L., Preusse, P., Oelhaf, H., Friedl-Vallon, F., and Riese, M.: Towards a 3-D tomographic retrieval for the air-borne limb-imager GLORIA, *Atmos. Meas. Tech.*, 3, 1647–1665, doi:10.5194/amt-3-1647-2010, 2010.
- Ungermann, J., Blank, J., Lotz, J., Leppkes, K., Hoffmann, L., Guggenmoser, T., Kaufmann, M., Preusse, P., Naumann, U., and Riese, M.: A 3-D tomographic retrieval approach with advection compensation for the air-borne limb-imager GLORIA, *Atmos. Meas. Tech.*, 4, 2509–2529, doi:10.5194/amt-4-2509-2011, 2011.
- Ungermann, J., Pan, L. L., Kalicinsky, C., Olschewski, F., Knieling, P., Blank, J., Weigel, K., Guggenmoser, T., Stroh, F., Hoffmann, L., and Riese, M.: Filamentary structure in chemical tracer distributions near the subtropical jet following a wave breaking event, *Atmos. Chem. Phys.*, 13, 10517–10534, doi:10.5194/acp-13-10517-2013, 2013.
- Vogel, B., Günther, G., Müller, R., Groß, J.-U., Bozem, H., Hoor, P., Krämer, M., Zahn, A., and Riese, M.: Contributions of different boundary layer sources in Asia to the Asian monsoon anticyclone and associated transport pathways to the lowermost Stratosphere over northern Europe in 2012, *Atmos. Chem. Phys.*, in preparation, 2014.
- Volk, C. M., Riediger, O., Strunk, M., Schmidt, U., Ravegnani, F., Ulanovsky, A., and Rudakov, V.: In situ Tracer Measurements in the Tropical Tropopause Region During APE-THESEO, *Eur. Comm. Air Pollut. Res. Report*, 73, 661–664, 2000.
- von Clarmann, T. and Echle, G.: Selection of optimized microwindows for atmospheric spectroscopy, *Appl. Optics*, 37, 7661–7669, 1998.
- von Clarmann, T., Höpfner, M., Kellmann, S., Linden, A., Chauhan, S., Funke, B., Grabowski, U., Glatthor, N., Kiefer, M., Schieferdecker, T., Stiller, G. P., and Versick, S.: Retrieval of temperature, H<sub>2</sub>O, O<sub>3</sub>, HNO<sub>3</sub>, CH<sub>4</sub>, N<sub>2</sub>O, ClONO<sub>2</sub> and ClO from MIPAS reduced resolution nominal mode limb emission measurements, *Atmos. Meas. Tech.*, 2, 159–175, doi:10.5194/amt-2-159-2009, 2009.
- Weigel, K., Hoffmann, L., Günther, G., Khosrawi, F., Olschewski, F., Preusse, P., Spang, R., Stroh, F., and Riese, M.: A stratospheric intrusion at the subtropical jet over the Mediterranean Sea: air-borne remote sensing observations and model results, *Atmos. Chem. Phys.*, 12, 8423–8438, doi:10.5194/acp-12-8423-2012, 2012.
- Werner, A., Volk, C. M., Ivanova, E. V., Wetter, T., Schiller, C., Schlager, H., and Konopka, P.: Quantifying transport into the Arctic lowermost stratosphere, *Atmos. Chem. Phys.*, 10, 11623–11639, doi:10.5194/acp-10-11623-2010, 2010.
- Woiwode, W., Oelhaf, H., Gulde, T., Piesch, C., Maucher, G., Ebersoldt, A., Keim, C., Höpfner, M., Khaykin, S., Ravegnani, F., Ulanovsky, A. E., Volk, C. M., Hösen, E., Dörnbrack, A., Ungermann, J., Kalicinsky, C., and Orphal, J.: MIPAS-STR measurements in the Arctic UTLS in winter/spring 2010: instrument characterization, retrieval and validation, *Atmos. Meas. Tech.*, 5, 1205–1228, doi:10.5194/amt-5-1205-2012, 2012.
- Woiwode, W., Suminska-Ebersoldt, O., Oelhaf, H., Hösen, E., Höpfner, M., Ebersoldt, A., Friedl-Vallon, F., Groß, J.-U., Gulde, T., Kaufmann, M., Kleinert, A., Krämer, M., Kretschmer, E., T. Kulesa, G. M., Piesch, C., Riese, M., Rongen, H., Sartorius, C., Schardt, G., Schönfeld, A., Schuettemeyer, D., Sha, M. K., Stroh, F., Volk, C. M., and Orphal, J.: Validation of first chemistry mode retrieval results from new limb-imaging FTS GLORIA with correlative MIPAS-STR observations, *Atmos. Meas. Tech. Discuss.*, submitted, 2014.